Article

HKUST-1-Supported Cerium Catalysts for CO Oxidation

Michalina Stawowy [1], **Paulina Jagódka** [1], **Krzysztof Matus** [2]**, Bogdan Samojeden** [3],
Joaquin Silvestre-Albero [4]**, Janusz Trawczyński** [1] **and Agata Łamacz** [1,*]

[1] Department of Chemistry and Technology of Fuels, Wrocław University of Science and Technology, Gdańska 7/9, 50-344 Wrocław, Poland; michalina.stawowy@pwr.edu.pl (M.S.); paulina.jagodka@pwr.edu.pl (P.J.); janusz.trawczynski@pwr.edu.pl (J.T.)
[2] Institute of Engineering Materials and Biomaterials, Silesian University of Technology, Konarskiego 18a, 44-100 Gliwice, Poland; krzysztof.matus@polsl.pl
[3] AGH University of Science and Technology, Al. A. Mickiewicza 30, 30-059 Kraków, Poland; bogdan.samojeden@agh.edu.pl
[4] Laboratorio de Materiales Avanzados, Departamento de Química Inorgánica-IUMA, Universidad de Alicante, Ctra. San Vicente-Alicante s/n, E-03690 San Vicente del Raspeig, Spain; joaquin.silvestre@ua.es
* Correspondence: agata.lamacz@pwr.edu.pl

check for updates

Abstract: The synthesis method of metal–organic frameworks (MOFs) has an important impact on their properties, including their performance in catalytic reactions. In this work we report on how the performance of $[Cu_3(TMA)_2(H_2O)_3]_n$ (HKUST-1) and Ce@HKUST-1 in the reaction of CO oxidation depends on the synthesis method of HKUST-1 and the way the cerium active phase is introduced to it. The HKUST-1 is synthesised in two ways: via the conventional solvothermal method and in the presence of a cationic surfactant (hexadecyltrimethylammonium bromide (CTAB)). Obtained MOFs are used as supports for cerium oxide, which is deposited on their surfaces by applying wet and incipient wetness impregnation methods. To determine textural properties, structure, morphology, and thermal stability, the HKUST-1 supports and Ce@HKUST-1 catalysts are characterised using X-ray diffraction (XRD), N_2 sorption, scanning electron microscopy (SEM), high-resolution transmission electron microscopy (HRTEM), X-ray photoelectron spectroscopy (XPS), Fourier transform infrared spectroscopy (FT-IR), and thermogravimetric analysis (TGA). It is proven that the synthesis method of HKUST-1 has a significant impact on its morphology, surface area, and thermal stability. The synthesis method also influences the dispersion and the morphology of the deposited cerium oxide. Last but not least, the synthesis method affects the catalytic activity of the obtained material.

Keywords: HKUST-1; surfactant; cerium oxide; CO oxidation

1. Introduction

HKUST-1, i.e., $[Cu_3(TMA)_2(H_2O)_3]_n$, is a metal coordination polymer which was reported for the first time in 1999 by Chui et al. [1]. In its framework, copper (II) ions form dimmers in which a single copper atom is coordinated with four oxygen atoms from the trimesic acid (H_3BTC) linker and H_2O molecules. Cubic crystal structures with a 3D system of pores which are characterised by a square shape and similar size (9×9 Å) are formed [2]. Usually, HKUST-1 is synthesised via the solvothermal method; however, to control crystal size and morphology, templates can be used. A common approach is to use monodentate ligands that have the same bond functionality as the linker. In such a case, the template (sometimes called the "modulator") competes with the organic linker to a metal ion and regulates at the same time the nucleation and crystal growth [3]. It has been found [4] that the addition of acetic acid leads to anisotropic growth of crystals, which physically prevents their aggregation.

Coordination modulators are used to obtain other metal–organic frameworks (MOFs) with different sizes and morphologies, including nHKUST-1 [5], nUiO-66 [6,7], nMOF-801 [8], and nZIF-8 [9]. In the case of HKUST-1, triethylamine (TEA) is frequently used as a template [10,11]. Materials prepared with TEA are nanocrystalline, e.g., their size can be decreased from 16 μm to 175 or 65 nm when the TEA:H_3BTC molar ratio is 1 or 3, respectively. This operation is slightly different than for classical templates because the use of TEA increases the pH of the solution and causes deprotonation of H_3BTC, facilitating its coordination to Cu^{2+} and speeding up the nucleation of HKUST-1 crystals [12].

The application of surfactants during MOF synthesis is also an important issue. It allows for controlling the size and growth of desirable crystalline material and conducting synthesis under milder conditions. Nune et al. [13] obtained nanosized ZIF-8 using high molecular weight poly(diallyldimethylammonium) chloride as a template. They maintained good thermal and chemical stability of the MOF. A no-ionic Pluronic F-127 surfactant (PF-127) was used as a controlling agent in the synthesis of rod-like HKUST-1 particles [14]. The growth mechanism of these particles assumed that the initially formed $Cu(H_2O)_6^{2+}$ ions were surrounded by PF-127 surfactant molecules that inhibited direct contact between Cu^{2+} ions and BTC ligands, preventing HKUST-1 crystallisation from occurring. Then, the H_2O ligands were exchanged with BTC ligands to form Cu-BTC crystals that worked as the crystallization nucleus. Further direction of HKUST-1 crystal growth was induced according to the specific adsorption of the PF-127 surfactant. Other coordination modulators used in HKUST-1 syntheses are polyacrylic acid (PPA) [15] and hexadecyltrimethylammonium bromide (CTAB). Long chain CTAB molecules are known to form micelles and vesicles under different situations [16]. Without CTAB, HKUST-1 crystals are cubic in their shape, with an average particle size of about 300 nm. In the presence of CTAB, the HKUST-1 morphology is changed. For example, Tan et al. [17] used CTAB to obtain ring-like HKUST-1 structures. It should be noted that the concentration of the surfactant, as well as the proper acid–base environment for the reaction that controls deprotonation of the organic linker, and, hence, the nucleation process, has an impact on the size of the HKUST-1 particles [17,18].

HKUST-1 has open copper sites which make it a reasonable candidate for catalytic applications. Unsaturated Cu^{2+} ions coordinate oxygen atoms, forming $μ_2$–oxygen bridges that inhibit saturation of the active centres. The open metal sites in MOFs are much more stable than in homogeneous systems [19]. HKUST-1 has already been used as a catalyst in a few reactions. For example, Yepez et al. [20] tested it in the reaction of oxidation of trans-ferulic acid to vanillin. HKUST-1 was found to be a very efficient catalyst in this reaction, providing a 98% acid conversion. It was found that the activation of HKUST-1 is crucial for the removal of H_2O, and, thus, generation of unsaturated metal sites, which is a key point for good catalyst performance. HKUST-1 has also been used as a catalyst in the synthesis of 1,4-dihydropyridine (1,4-DHP), a compound that possesses important biological and pharmaceutical properties. Arzehgar at al. [21] have reported one-pot synthesis of 1,4-DHP in EtOH with an excellent (95%) yield in the presence of HKUST-1. Toyao et al. [22] describe examples of catalysts which consist of nanoparticles loaded onto HKUST-1. Fe_3O_4@HKUST-1 and Pd/Fe_3O_4@HKUST-1 have been used for one-pot deacetalisation and Knoevenagel condensation reactions as well as in the hydrogenation of olefins. Guo et al. [23] have studied HKUST-1 in bimetallic catalysts [$Cu_{3-x}Pd_x(BTC)_2$]. They found that incorporation of Pd^{2+} into Cu nodes in HKUST-1 allowed for the obtaining of catalysts with unsaturated palladium centres. They also proved that the catalyst contained some amounts of Cu^+. The obtained catalyst was found to be very active in alcohol oxidation, allylic oxidation and rearrangements, cycloisomerisation, and olefin hydrogenation. It was also used in the selective oxidation of benzyl alcohol to benzaldehyde. HKUST-1-supported catalysts are promising materials for CO oxidation to CO_2. HKUST-1 and Pd@HKUST-1 have been reported by Ye et al. [24] to reveal 100% conversion of CO to CO_2 at 240 and 220 °C, respectively. It was observed by these authors that Pd presence improves HKUST-1 activity and decreases the temperature of CO maximal conversion. It was also observed that HKUST-1 lost its crystallinity after impregnation with Pd, but the structural collapse arising from the cleavage of coordination bonds was said to contribute to the improvement of catalytic activity of the material, owing to the increased number of unsaturated Cu cation coordination sites active for CO

oxidation. Owing to the very good redox properties of ceria, the bimetallic Ce–Cu system is a good alternative for noble metals. Zamaro et al. [25] have reported a 100% CO conversion over HKUST-1 at 240 °C. The HKUST-1 itself was not very active as a catalyst but it was found to be a good matrix for obtaining a CuO–CeO$_2$ system of improved performance in CO oxidation compared to the initial material (100% CO conversion was achieved at 150 °C).

In this work we show the catalytic activity of HKUST-1 and Ce@HKUST-1 materials in the reaction of CO oxidation. Our aim was to obtain a Ce–Cu system and employ the best features of HKUST-1 (including its developed surface area, porosity, and the presence of open Cu sites) together with the already mentioned advantages of cerium. Cerium–copper oxide mixtures have recently shown increased importance for oxidation catalysis [26]. In this work we obtain HKUST-1 using (i) conventional solvothermal synthesis and (ii) a CTAB-assisted procedure. Both MOFs are later impregnated with cerium salt to obtain a bimetallic Ce–Cu catalyst, preserving the original HKUST-1 framework.

2. Results and Discussion

2.1. Characterisation

Figure 1 presents the XRD results for obtained HKUST-1 (i.e., H1 and H1_CTAB) and Ce@HKUST-1 samples (i.e., Ce@H1(W), Ce@H1(D), Ce@H1_CTAB(W), and Ce@H1_CTAB(D), where W and D stand for samples obtained via wet and incipient wetness impregnation, respectively). The diffraction peaks at 6.6, 9.4, 11.5, and 13.4° correspond to the (200), (220), (222), and (400) crystal planes, respectively. It can be observed that the position of these reflexions is the same when HKUST-1 is synthesised with CTAB (H1_CTAB) and after impregnation of both HKUST-1 supports with cerium nitrate. Hence, neither the addition of the CTAB template during synthesis nor the impregnation process damaged the HKUST-1 framework. The particles sizes calculated for (200), (220), (222), and (400) reflexions are presented in Table 1. In addition, no peaks of cerium phase are observed.
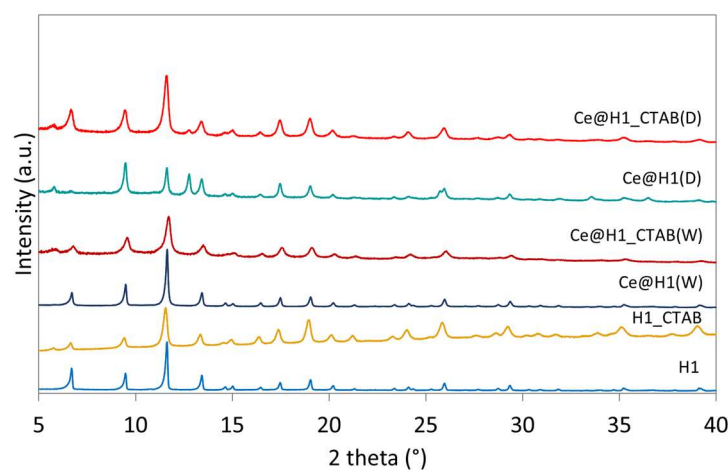

Figure 1. XRD of HKUST-1 and Ce@HKUST-1 materials (descriptions for sample names are given in Materials and Methods, i.e., in Sections 3.1 and 3.2).

The specific surface area (S$_{BET}$) of HKUST-1 and Ce@HKUST-1 was calculated from N$_2$ adsorption/desorption isotherms. The shape of each plot presented in Figure 2 indicates a Type I isotherm according to the IUPAC classification, which is typical for microporous materials. The hysteresis loop observed for H1 and Ce@H1(W) at a relative pressure P/P$_0$ > 0.4 indicates the capillary condensation in mesopores whose presence can arise from the stacking of larger particles of HKUST-1 or the formation of defects in the HKUST-1 framework. It was also confirmed with the N$_2$ sorption experiments that the total pore volume was similar for both H1 and Ce@H1(W) (Table 2). The textural properties of the HKUST-1 and Ce@HKUST-1 materials are presented in Figure 2. Pure HKUST-1 had

S_{BET} of 1003 m^2/g, whereas the addition of CTAB to the synthesis as well as impregnation with cerium nitrate led to a decrease in the surface area which arose from the blockage of pores and the coverage of HKUST-1 crystals with the cerium phase. The most severe decrease in S_{BET} was observed when the synthesis of HKUST-1 was carried out in the presence of CTAB (H1_CTAB); this was caused by the insufficient removal of CTA$^+$ cations from the sample. The impregnation of that material with cerium nitrate, followed by thermal activation at 160 °C, helped to remove the CTA$^+$ from the sample, resulting in an increase in S_{BET} in the case of Ce@H1_CATB(W) and Ce@H1_CTAB(D). Moreover, impregnation of H1_CTAB resulted in an increase in the mean pore size (d) because it facilitated the removal of the remaining CTA$^+$ ions, and this led to formation of large-scale defects in the HKUST-1 particles.

Table 1. Particle size for HKUST-1 and Ce@HKUST-1 materials calculated for (200), (220), (222), and (400) reflexions.

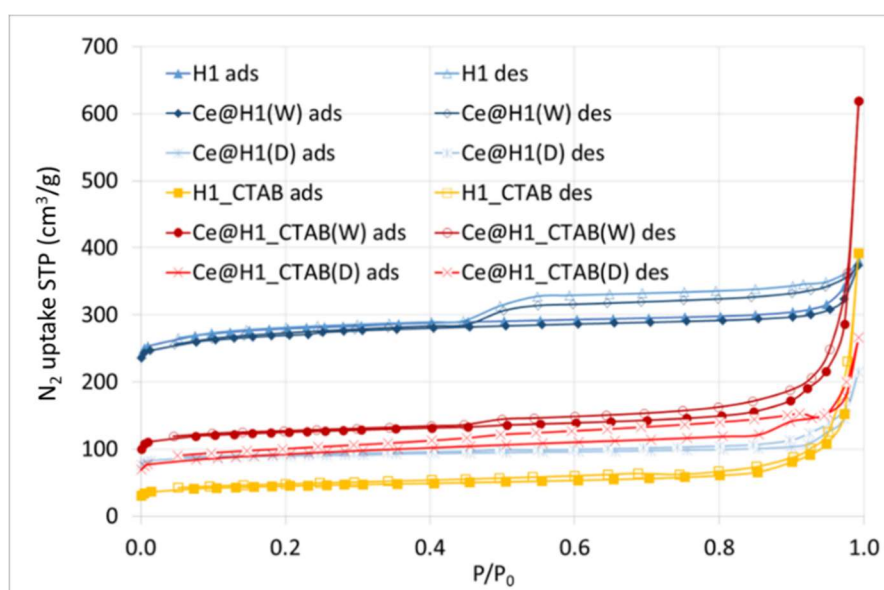| Crystal Plane	Particle Size (nm)					
	H1	H1_CTAB	Ce@H1(D)	Ce@H1_CTAB(D)	Ce@H1(W)	Ce@H1_CTAB(W)
(200)	429.1	504.9	233.6	302.9	237.6	253.9
(220)	453.5	318.6	364.5	227.5	818.7	226.6
(222)	473.9	358.6	565.7	220.7	713.5	278.0
(400)	469.9	290.2	268.2	287.5	748.6	218.7

Figure 2. N$_2$ adsorption–desorption isotherms at standard temperature and pressure (STP) for HKUST-1 and Ce@HKUST-1 materials. "Ads"—adsorption, "des"—desorption.

Table 2. Textural properties of HKUST-1 and Ce@HKUST-1 materials: specific surface area (S_{BET}), total pore volume (V_{total}), and mean pore size (d).

Sample	S_{BET} (m^2/g)	V_{total} (cm^3/g)	d (nm)
H1	1003	0.584	2.3
Ce@H1(W)	958	0.574	4.2
Ce@H1(D)	318	0.331	4.2
H1_CTAB	160	0.602	1.5
Ce@H1_CTAB(W)	444	0.952	8.6
Ce@H1_CTAB(D)	328	0.409	5.0

The morphology of HKUST-1 and Ce@HKUST-1 and the dispersion of the cerium phase over HKUST-1 was observed with scanning and high-resolution transmission electron microscopy (SEM and HRTEM) (Figures 3–6). It can be seen in Figure 3a that the size of the octahedral particles of HKUST-1 obtained via the solvothermal method (H1) is uneven and ranges from around 5 to 20 µm. SEM pictures also show the pores in the H1 material, including after its wet impregnation with cerium nitrate (Figure 3b,d). It can be seen that the cerium phase formed spherical CeO_2 particles of a diameter ranging from around 200 nm to 1 µm that dispersed over HKUST-1. The incipient wetness impregnation of H1 with cerium nitrate (Ce@H1(D)) led to the uniform coverage of HKUST-1 particles with CeO_x rods [27] of 200 nm–2 µm length (Figure 3e,f). The Ce_2O_3 presence in the Ce@H1(D) sample was detected by the selected area electron diffraction (SAED) (Figure 4b). Blocking of the porous surface of the HKUST-1 with the cerium phase caused a significant decrease in S_{BET} and V_{total} when compared to H1 and Ce@H1(W) (Table 2). In both samples the nanocrystals of cerium oxide were distributed over HKUST-1 but also formed agglomerates detached from the MOF (Figure 4).
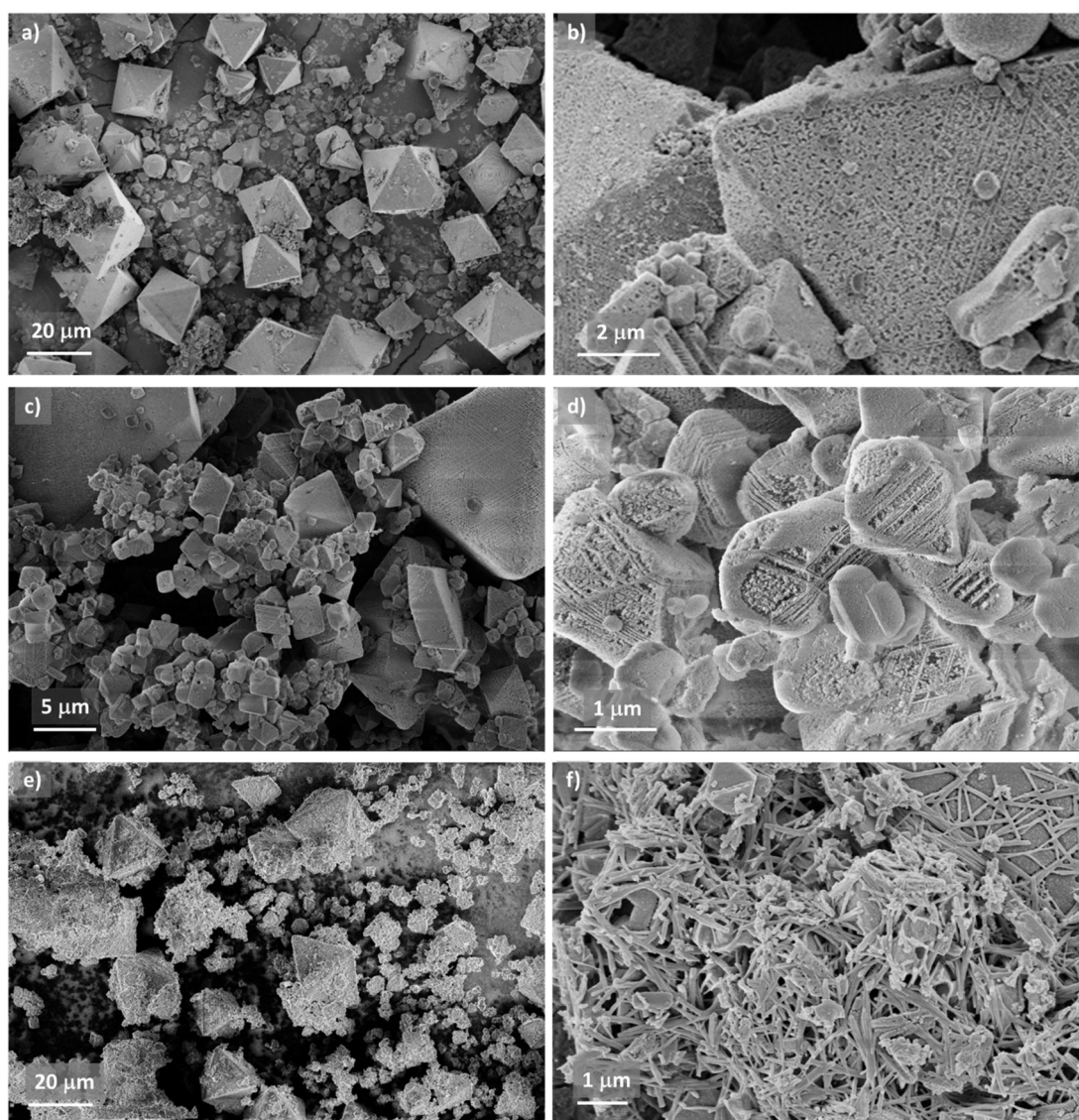

Figure 3. Morphology of H1 (**a**,**b**), Ce@H1(W) (**c**,**d**), and Ce@H1(D) (**e**,**f**).
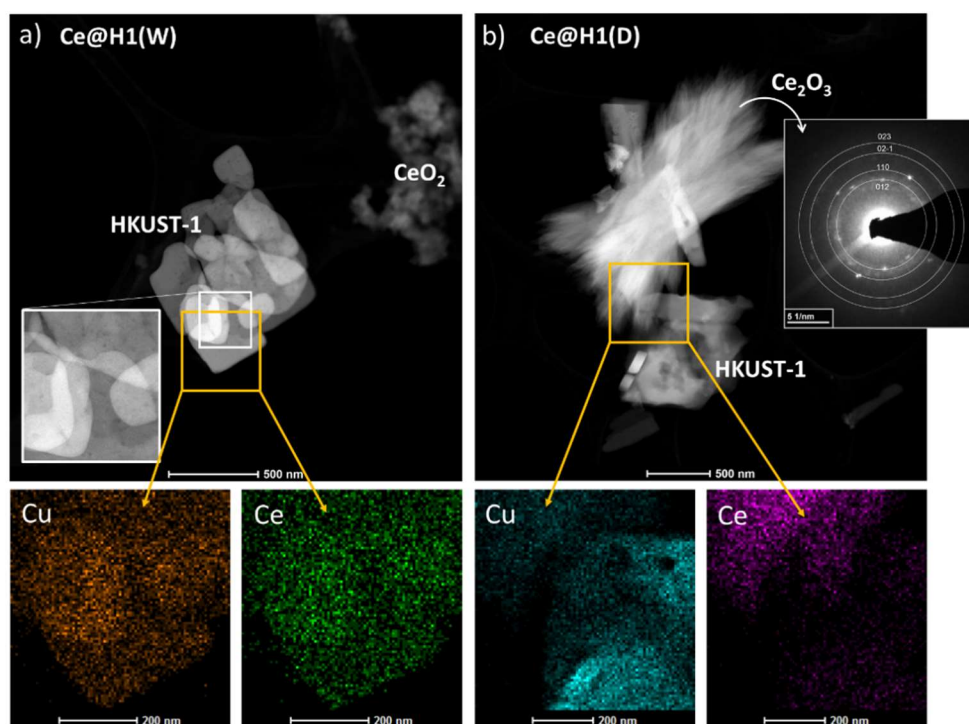
Figure 4. High-angle annular dark-field imaging (HAADF-STEM) images of Ce@H1(W) (**a**) and Ce@H1(D) (**b**) with marked area of Cu and Ce EDS maps. The SAED electron diffraction of Ce_2O_3 in Ce@H1(D) is shown on the right side of (**b**).
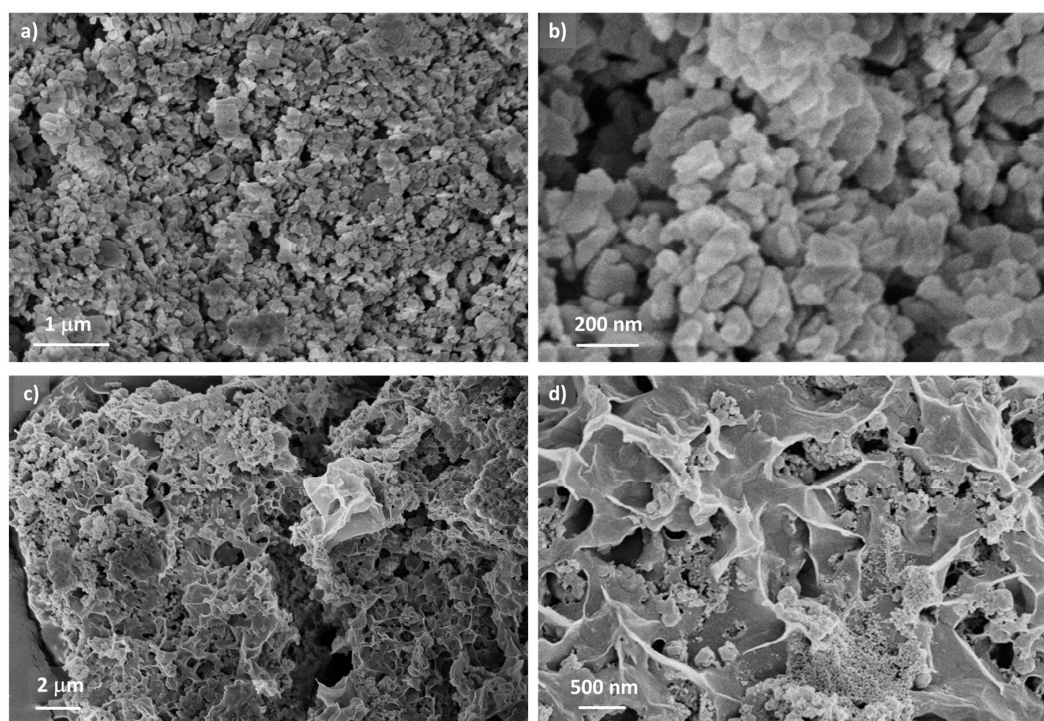

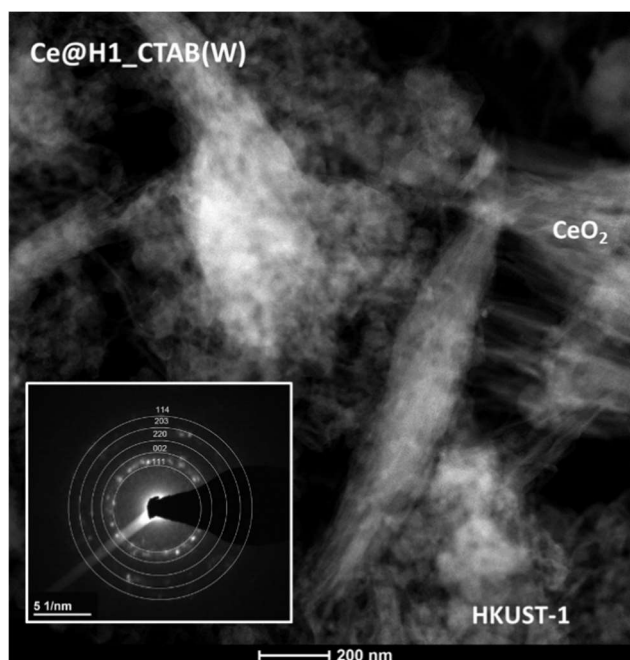**Figure 5.** Morphology of H1_CTAB (**a**,**b**) and Ce@H1_CTAB(W) (**c**,**d**).

Figure 6. HAADF-STEM image of Ce@H1_CTAB(W) with SAED electron diffraction of CeO_2 phase.

The CTAB-assisted synthesis (H1_CTAB) resulted in the formation of smaller HKUST-1 particles with a diameter of up to 100 nm that were more spherical in shape. Tan et al. [17] used CTAB to obtain a hierarchical ring-like HKUST-1. This allowed for an increase in the mesoporosity and anionic properties of that MOF. In our case, the ring-like structures did not occur in the H1_CTAB sample (Figure 5a,b), but this may have been due to insufficient removal of CTAB during the washing step. Additionally, the temperature of thermal activation of the H1_CTAB samples was too low for thermal decomposition of CTAB, which takes place at 200–250 °C [28]. Successful removal of CTA^+ from HKUST-1 makes the MOF anionic, facilitating the introduction of another metal cation to the framework and providing good dispersion of that metal. In contrast to Tan et al. [17], who exchanged CTA^+ with Co, Ni, and Ce, etc., the impregnation of obtained in this work the H1_CTAB with cerium nitrate resulted in the formation of thin, irregularly-shaped sheets around small HKUST-1 particles (Figure 5c,d) that formed a kind of sponge. According to the SAED and energy-dispersive X-ray spectroscopy (EDS) performed during the HRTEM examination of that sample, that sponge-like structure was CeO_2 (Figure 6). Also, it can be observed in Figure 3d that some of the HKUST-1 particles in Ce@H1_CTAB(W) have a ring-like shape, which evidences the elimination of CTAB molecules. Chitsaz et al. [29] studied the impact of CTAB on nano-CeO_2 crystallisation via the co-precipitation method using cerium (III) nitrate hexahydrate as the Ce precursor. Obtained CeO_2 nanoparticles of around 5 nm in diameter possessed a cubic fluorite structure. Kim et al. [30] synthesised micro-sponges of CeO_2–CuO (6 wt.% Cu) nanoparticles by mixing aqueous nitrate solutions of Ce and Cu with natural biopolymers (dextran and xyloglucan). In their method the freeze drying of the metal oxide–dextran mixture was applied as a first step which allowed for the forming of porous monoliths and minimised crystal sintering during the subsequent step of heating the obtained material at 600 °C. During wet impregnation the H1_CTAB was suspended in EtOH, which probably resulted in the removal of the CTA^+ from the inside of the HKUST-1 particles. In the ethanolic solution CTAB interacted with $Ce(NO_3)_3$, whereas during heating the O_2 and NO_x that desorbed from nitrates accelerated the combustion of CTAB. Pan et al. [31] have reported that the Ce^{3+}/CTAB ratio as well as the synthesis temperature and duration influence the morphology of obtained CeO_2. At a lower temperature, nanoplates are formed and their geometry changes from irregular to hexagonal when the temperature increases to 140 °C. The CTAB absorbs on the exposed surface of CeO_2 crystal and limits its growth. The increase in reaction time results in the transformation

of nanoplates to nanorods. In our case, the reaction time was relatively short, i.e., 3 h, which explains the formation of CeO_2 thin sheets.

SEM and TEM revealed that cerium dispersion over H1 was less uniform than in the case of H1_CTAB. Hence, cerium deposition over HKUST-1 obtained in the presence of CTAB is more efficient. This may be due to some exchange of CTA^+ to Ce^{3+}, according to the mechanism described in [17].

Determination of the electronic properties of the prepared HKUST-1 and Ce@HKUST-1 catalysts was performed with X-ray photoelectron spectroscopy (XPS). The peak fitting of high-resolution C 1s, O 1s, Cu 2p, and Ce 3d (Figure 7) allowed for a comparison of the chemical states of C, O, Cu, and Ce in the modified HKUST-1 samples. The fitted XPS spectra of Cu 2p consists of a few peaks and shows domination of the divalent Cu. The Cu $2p_{3/2}$ and Cu $2p_{1/2}$ peaks of Cu^{2+} are located at around 934 and 954 eV, respectively, with a shake-up satellite at around 944 eV. The presence of Cu^+ is confirmed by peaks at around 932 and 952 eV [32]. In order to further investigate the valence state of copper and differentiate between Cu^+ and Cu^0, CuLMM spectra were recorded for all samples. The CuLMM Auger peaks (Figure 8) occur at around 571.5 eV, which indicates the presence of Cu^+ ions. Normally, the Auger peak of Cu^0 is about 2 eV lower than for Cu^+, but the CuLMM spectra do not show band broadening to lower binding energies. Hence, we may assume that Cu^0 was not present in the sample.

The Cu^{2+}/Cu^+ ratio in the obtained samples was found to be as follows: 2.39 for H1, 1.75 for H1_CTAB, 1.69 for Ce@H1(W), 1.55 for Ce@H1_CTAB(W), 1.63 for Ce@H1(D), and 1.60 for Ce@H1_CTAB(D). Hence, the Cu^{2+} ions were found to predominate over Cu^+ in all the samples, but the contribution of the latter increased after CTAB use in the synthesis of HKUST-1 and after Ce deposition. A higher concentration of Cu^+ than in the case of conventional HKUST-1 (H1) can be said to be due to an oxygen transfer from Cu^{2+} to Ce^{3+}, leading to reduction/oxidation to Cu^+ and Ce^{4+}, respectively. This may indicate strong interactions between Cu nodes in HKUST-1 with deposited Ce species.

The C 1s spectra show a few peaks at binding energies of around 284.6, 288, and 288.8 eV, which correspond to C–C/C=C, C=O, and O=C–O bonds in trimesic acid [33]. The peaks assigned to O–C=O and C=O are shifted to higher binding energies after H1 and H1CTAB impregnation with cerium. Modification of HKUST-1 either by the addition of CTAB or cerium decreases the amount of the deprotonated carboxylic groups; the concentration of pendant $O–C=O^-$ decreases from 16.87 to 7.41 at.% and from 6.93 to 6.86 at.% after impregnation of H1 and H1_CTAB, respectively. The peak at around 285.5 eV can be attributed to a C-N bond and its occurrence indicates the presence of N,N-dimethylformamide (DMF) in the HKUST-1 pores [34].

The O 1s spectra shows three oxygen species, i.e., the C−O−Cu in the paddle-wheel secondary building units (SBU) at around 531.5 eV, the O–C=O of the trimesic acid at around 532.6 eV, and the O–H at around 533.8 eV [35,36]. The energy of the Ce^{3+}—O bond can occur at around 531.7 eV.

The Ce 3d XPS spectra show few peaks that are characteristic of the +3 and +4 oxidation states of cerium of CeO_x. There is no artificial increase in the Ce^{3+} concentration because samples were not subjected to Ar sputtering, causing oxygen scavenging. Normally, the existence of Ce^{3+} and Ce^{4+} is evidenced by doublets that are bound together, and their splitting is at around 18.4 eV. The Ce^{3+} presence is also shown by three singlets [37]. In the presented case, the peaks corresponding to Ce^{3+} predominate, whereas only two doublets for Ce^{4+} are observed. The Ce^{3+}/Ce^{4+} ratio was found to be 1.69 for Ce@H1(W), 1.62 for Ce@H1(D), 1.66 for Ce@H1_CTAB(W), and 1.63 for Ce@H1_CTAB(D). Hence, there is no significant difference in the contribution of both species in all samples and one may conclude that neither the CTAB application for HKUST-1 synthesis nor the impregnation method influence the Ce oxidation state.

The FTIR spectra of HKUST-1 and Ce@HKUST-1 are shown in Figure 9. All spectra in the 2000–400 cm^{-1} region display bands at the same wavenumber. The bands below 1200 cm^{-1} are assigned to the vibrations of the BTC linker, whereas bands in the 1700–1300 cm^{-1} region correspond to the BTC linker coordinated to the copper sites (the asymmetric and symmetric stretching vibrations of the carboxylate in BTC are observed at around 1650 cm^{-1} and 1374 cm^{-1}, respectively) [38,39].

The IR band at 1440 cm^{-1} can be ascribed to C=O of uncoordinated H$_3$BTC [40]. In addition, on the FTIR spectra of H1_CTAB and Ce@H1_CTAB(D) there are low intensity bands at 2853 and 2923 cm^{-1} (Figure 9a) that correspond to the symmetric and asymmetric stretching modes of CH$_2$ coming from trapped CTA$^+$ species [17].
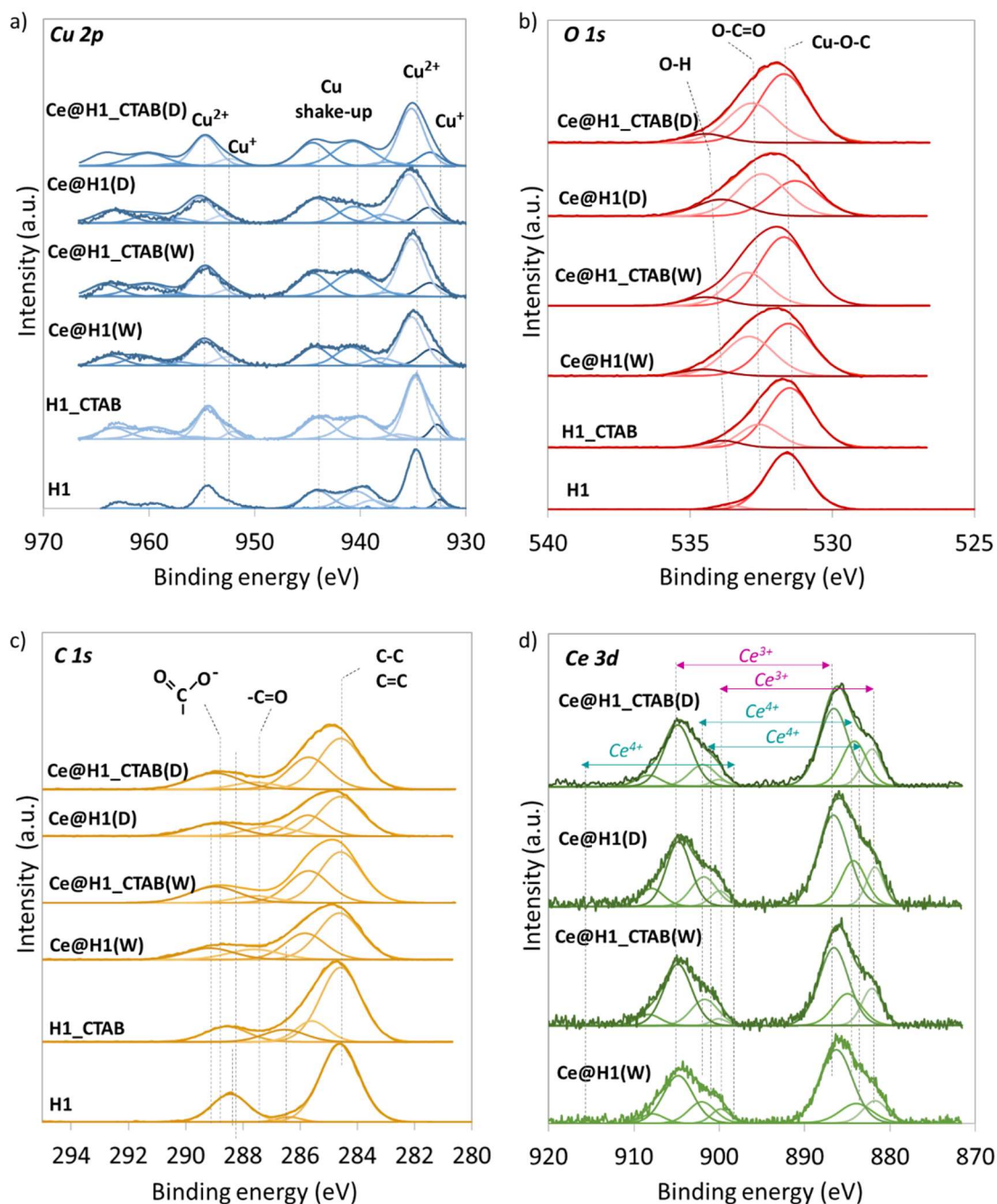

Figure 7. XPS Cu 2p (**a**), O 1s (**b**), C 1s (**c**) and Ce 3d (**d**) spectra of HKUST-1 and Ce@HKUST-1 materials.
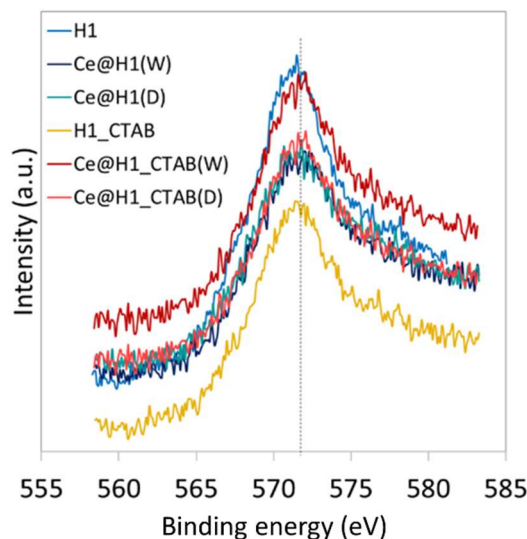
Figure 8. CuLMM Auger spectra for HKUST-1 and Ce@HKUST-1 materials.
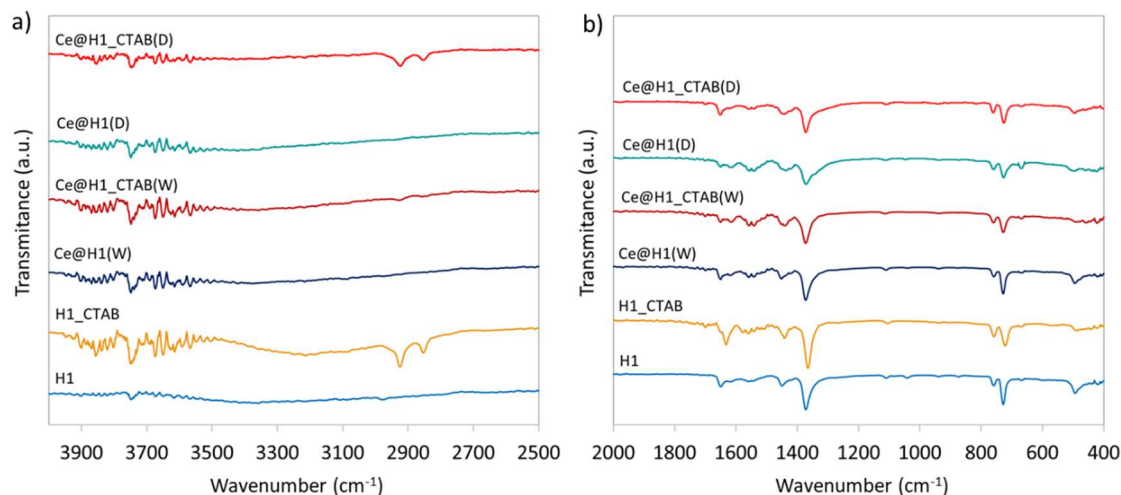

Figure 9. FTIR spectra of HKUST-1 and Ce@HKUST-1 materials in the 4000–2500 cm^{-1} (**a**) and 2000–400 cm^{-1} (**b**) range.

The results of TGA for the obtained materials are presented in Figure 10. The first mass loss up to 110 °C can be ascribed to the evaporation of physically adsorbed water. It is known that HKUST-1 easily adsorbs water, and it can be removed from the sample via heating at around 110 °C. A further mass decrease at up to around 300 °C for HKUST-1 obtained via solvothermal synthesis and its Ce-containing counterparts, and up to around 250 °C for HKUST-1 and Ce/HKUST-1 obtained with CTAB, is due to evaporation of H_2O that was chemically adsorbed on the Cu atoms or the solvent that remained in the HKUST-1 pores. In the case of the H1_CTAB sample, a rapid mass loss of 4.2% can be observed at 240–260 °C. This may be attributed to the thermal decomposition of unwashed CTAB. The TGA profiles for cerium-containing samples (Ce@H1_CTAB(W) and Ce@H1_CTAB(D)) do not show a mass loss in that region because the residual CTAB was removed from HKUST-1 upon extended washing after impregnation with cerium nitrate. That is also the reason for the higher S_{BET} of the Ce@H1_CTAB compared to H1_CTAB (444 m^2/g versus 160 m^2/g, Table 2).
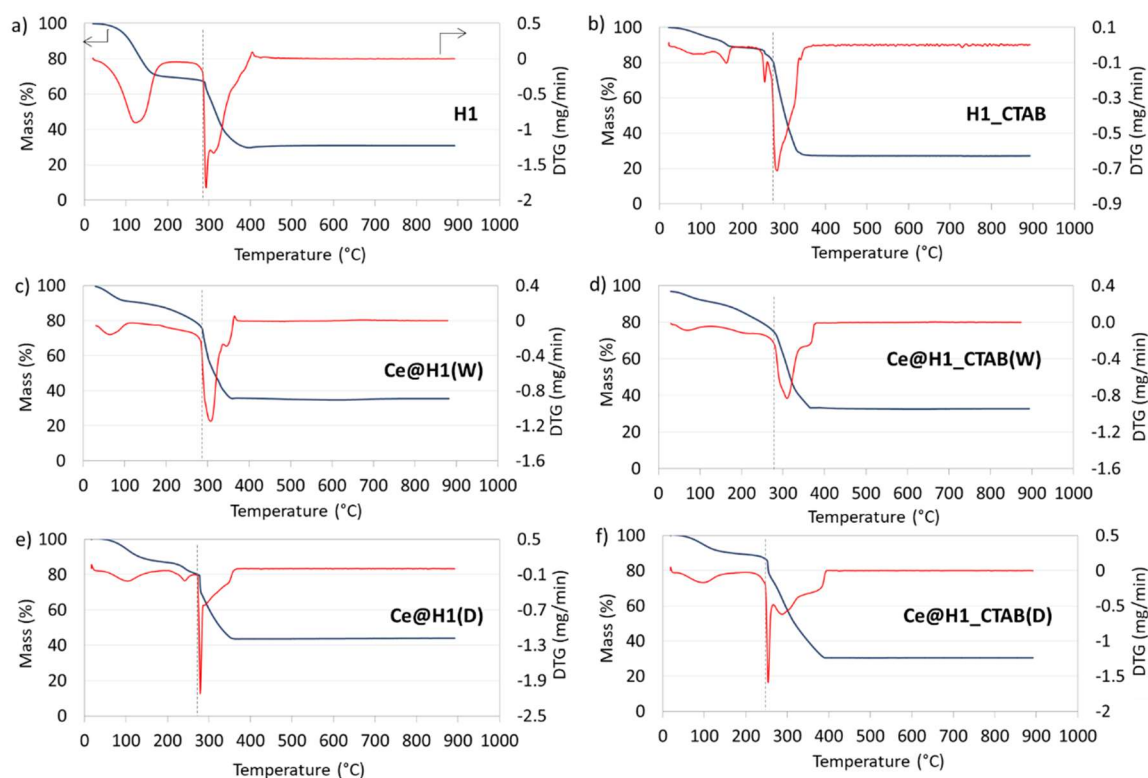
Figure 10. Mass of the sample (blue) and DTG (red) plots for HKUST-1 (**a**,**b**) and Ce@HKUST-1 materials (**c**–**f**).

The obtained samples are characterised with different thermal stability. The framework of HKUST-1 obtained in solvothermal synthesis (H1) was found to be stable up to 286 °C, whereas the material obtained with the template (H1_CTAB) started to decompose at a temperature lower than this by 15 °C (Table 3). Impregnation with cerium nitrate decreased the thermal stability of all samples but the effect of cerium was more pronounced for Ce@H1_CTAB(W) and Ce@H1_CTAB(D). The total mass decrease owing to BTC linker decomposition was about 36% for H1 and Ce@H1, which is a typical value for those materials. A significantly higher, over 52% mass decrease was observed for the H1_CTAB and Ce@H1_CTAB samples and was due to the presence of metal cluster vacancies. In the CTAB-assisted synthesis the cationic surfactant (CTA^+) coordinates to BTC^{3-} instead of Cu^{2+}, thus producing larger structure defects.

Table 3. Temperature of structure decomposition and mass loss due to combustion of BTC linker.

Sample	Temperature of Decomposition (C)	Mass Loss (%)
H1	286	36.8
Ce@H1(W)	270	36.1
Ce@H1(D)	271	35.8
H1_CTAB	261	56.4
Ce@H1_CTAB(W)	235	52.1
Ce@H1_CTAB(D)	229	57.9

2.2. Catalytic Tests of CO Oxidation

The HKUST-1 and Ce@HKUST-1 catalysts were tested in the reaction of CO oxidation. The results of the catalytic tests are presented in Figure 11. It can be observed that the samples obtained with the use of the CTAB template reveal significantly lower CO conversions than their analogues synthesised via the solvothermal route. The best catalytic performance was shown for Ce@H1(D) which was active from 150 °C and provided 100% conversion of CO at 200 °C. Its analogue obtained via wet impregnation,

i.e., Ce@H1(W), required a significantly higher temperature for converting CO to CO_2 (above 180 °C), which could have been caused by the poorer coverage of HKUST-1 with CeO_x, and thus the reduced number of sites of strong Cu–Ce contact. It was proven by microscopic observations that Ce@H1(D) was well covered with the CeO_x phase; this (not the specific surface area) is the most important factor when speaking of the catalytic activity of Ce@HKUST-1 materials. Both Ce@H1(W) and Ce@H1(D) provided 100% CO conversion at lower temperatures than those reported in [24]. Similarly, CO oxidation to CO_2 over materials obtained in CTAB-assisted synthesis was also observed above 180 °C, but the maximal CO conversions were as low as 8 and 3.5% for H1_CTAB and Ce@H1_CTAB(W), respectively. Ce@H1_CTAB(D) showed a much better performance than the other two materials. It must also be mentioned that each catalyst decomposed in a CO/O_2/Ar mixture when the temperature exceeded the maximal value marked on the plot. H1 was revealed to have the highest thermal stability under the reaction conditions. The introduction of CeO_x to the catalytic system decreased the thermal resistance of the catalysts. Both the H1- and H1_CTAB-supported cerium catalysts were thermally stable up to 200 °C. Only H1_CTAB decomposed at above 190 °C, which was probably due to combustion of CTA^+, followed with thermal degradation of BTC linker molecules coordinated to CTA^+.
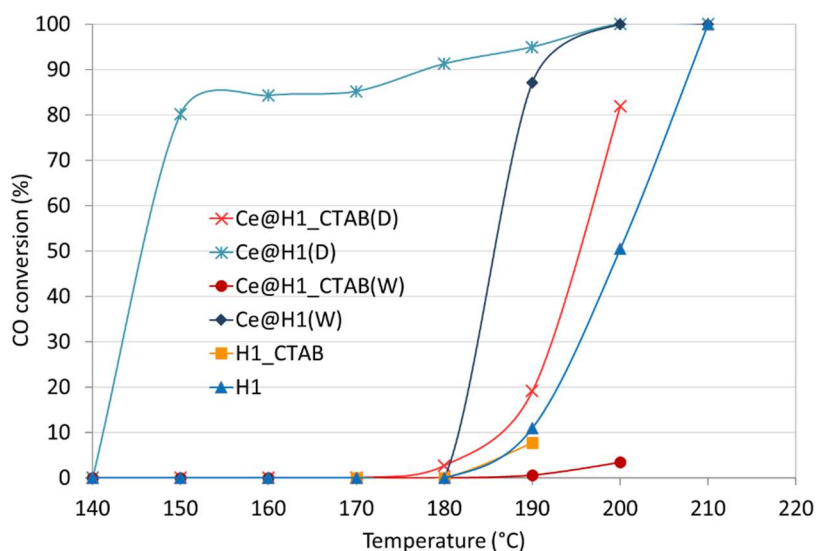

Figure 11. CO conversion versus temperature over HKUST-1 and Ce@HKUST-1 catalysts.

In contrary to other works on CO oxidation over MOF-based catalysts that undergo in situ transformation to CeO_2–CuO [25,41], our aim was to conduct the reaction maintaining the metal–organic framework. It was proven by the XRD analysis for H1, Ce@H1(W), and Ce@H1(D) (Figure 12) that after catalytic tests the HKUST-1 structure was preserved; however, small intensity reflexes of CuO and Cu_2O can be observed on the diffractogram of H1, which is due to oxidation of the BTC linker.

For example, Zamaro et al. [25] reported that HKUST-1 itself was not active in CO oxidation but that it was found to be a good matrix for obtaining well-dispersed CuO nanoparticles. In addition, incorporation of Ce and further activation of the material resulted in a highly dispersed bimetallic system of strong CeO_2–CuO interactions that improved CO oxidation when compared to HKUST-1-derived CuO alone. Over the Ce-HKUST-1-derived CeO_2–CuO, total CO conversion was achieved at 150 °C. Guo et al. [41] obtained CeO_2–CuO bimetallic catalysts derived from Cu supported on Ce–MOF–808 which showed 100% CO conversion above 300 °C, which is a significantly higher temperature than in the case of that reported in this work for HKUST-1-based catalysts. Zhu et al. [42] synthesised Ce-UiO-66-derived CuO–CeO_2 catalysts and studied them in preferential CO oxidation (PROX). Total CO conversion was achieved at 112 °C. It is known [43] that the Cu–Ce–O system is very active for complete oxidation of CO, with catalytic activity comparable to that of Pt-based catalysts. In the Cu–Ce system, the Cu^+ species are centres for CO adsorption and are stabilised by interactions between CuO

and CeO_2, whereas ceria provides the oxygen. The redox cycles occurring in Cu^{2+}/Cu^+ and Ce^{3+}/Ce^{4+} pairs in the CeO_2–CuO mixture are extremely important for the performance of the catalyst. However, the CeO_2–CuO interaction is also dependent on the synthesis method of such a system [44].
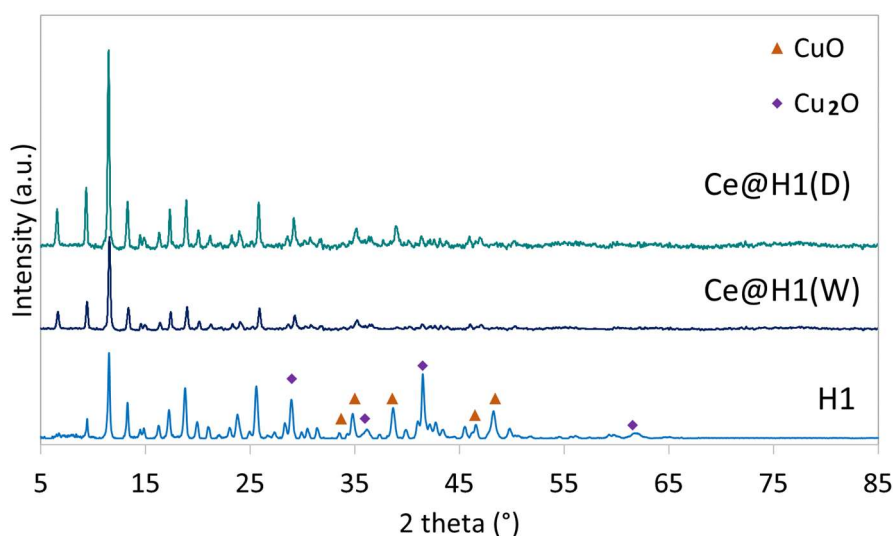

Figure 12. XRD for HKUST-1 and Ce@HKUST-1 catalysts after tests of CO oxidation.

MOFs and MOF-supported catalysts have great potential in heterogeneous catalysis because of their exceptional electronic types and their ability to promote the capture and activation of reagents or intermediates. The nodes in MOFs are active sites in redox processes; hence, their geometry and accessibility (i.e., open metal sites (OMS)) are key factors in catalytic performance. The co-adsorption of CO and O_2 over HKUST-1 and MOF-14 has been studied in situ by using ultrahigh vacuum infrared spectroscopy (UHV-FTIRS) [45]. It was found that CO adsorbed at the intrinsic Cu^{2+} coordinatively unsaturated sites (CUS) at $-168\ °C$ and that its oxidation to CO_2 occurred even at this low temperature. According to the proposed mechanism, two CO molecules adsorbed at the same time over two adjacent CUS, forming $CO–Cu^{2+}$. The catalytic reaction occurred only in the case of CO pre-adsorption, which facilitated activation of O_2 species. No intermediate products were observed to be formed; hence, it was assumed that O_2 molecules reacted directly with adsorbed CO to give CO_2. However, the CO adsorption over the metal nodes in MOFs should be considered complex because, as was reported by Noei et al. [46], more than one thermally stable CO species characterised by different binding energies can adsorb on unsaturated coordination sites in mixed-valence MOF.

3. Materials and Methods

3.1. Synthesis of HKUST-1

Synthesis of HKUST-1. Copper (II) nitrate trihydrate (5.0731 g) and trimesic acid (2.5281 g) were dissolved in DMF (62.5 mL) and ethyl alcohol (62.5 mL). The mixture was sonicated for 10 min until a blue suspension was obtained. The solution was placed in an oven and heated at 120 °C for 24 h. The blue product was filtered off under vacuum and washed with DMF (130 mL) and ethanol (200 mL). The obtained product, denoted **H1**, was dried at 60 °C for 12 h.

Synthesis of HKUST-1 with CTAB. The synthesis was conducted according to Tan et al. [17]. In the first flask, to deionised water (72 mL) a 0.11 M solution of trimesic acid (H_3BTC, 8.4 mL) was added. Next, triethylene amine (1.82 mL) was instilled and the mixture was stirred for 30 min. In the second flask, 0.5 M aqueous solution of copper (II) nitrate trihydrate (1.13 mL) was mixed with 0.1 M hexadecyltrimethylammonium bromide (CTAB, 48 mL) and H_2O (30 mL). The contents of both flasks were mixed together and stirred for 30 min at room temperature. The obtained green product was

filtered, washed with ethanol and dried at 60 °C for 12 h. The synthesised material was denoted **H1_CTAB**.

3.2. Synthesis of Ce@HKUST-1

Synthesis of Ce@HKUST-1 via wet impregnation. The H1 or H1_CTAB (1 g) was suspended in ethanol (190 mL) and stirred for 5 min. Next, a methanolic solution of 0.1 M cerium (III) nitrate hexahydrate (10 mL) was slowly instilled and the mixture was stirred for 3 h. The obtained product was filtered under vacuum and washed with ethanol. The obtained products, denoted **Ce@H1(W)** and **Ce@H1_CTAB(W),** were dried at 160 °C for 12 h. The nominal loading of cerium in both samples was 10 wt.%.

Synthesis of Ce@HKUST-1 via incipient wetness impregnation (IWI). To H1 (1 g) or H1_CTAB (0.2 g) an ethanolic solution of cerium (III) nitrate hexahydrate was slowly instilled and stirred continuously. Next, the homogeneous mixture was left to dry overnight at room temperature. Then, it was dried at 160 °C for 12 h. The obtained materials were denoted **Ce@H1(D)** and **Ce@H1_CTAB(D)**. The nominal Ce loading in both samples was 10 wt.%.

3.3. Characterisation

Powder X-ray diffraction analyses were performed from 5 to 80° with a 0.03° step using an X'Pert Pro apparatus (PANalitycal, Malvern, UK) which had Ni-filtered Cu Kα radiation (λ = 1.54056 Å) and was equipped with specific optics for performing analysis by small-angle X-ray scattering (SAXS) in transmission geometry. The X'Pert HighScore Plus program was used for results analysis.

N_2 *adsorption* at 77 K was performed using an Autosorb 1C (Quantachrome Instruments, Boynton Beach, FL, USA). Before tests the sample was outgassed in a vacuum at 100 °C for 12 h. The specific surface area was determined using the multipoint BET method and the total pore volume was estimated from the N_2 uptake at a relative pressure of P/P_0 = 0.99.

X-ray photoelectron spectroscopy was performed using a Thermo-Scientific K-ALPHA (Waltham, MA, USA) spectrometer equipped with Al-K radiation (1486.6 eV). The hemispherical analyser was run in constant energy mode with survey scan pass energies of 200 eV for measuring the whole energy band and 50 eV in a narrow scan for selective measuring of particular elements. The background subtraction and fitting of the experimental curve to a combination of Lorentzian (30%) and Gaussian (70%) lines was performed. The binding energies were referenced to the C 1s line at 284.6 eV and had an accuracy of ± 0.1 eV.

Microscopic observations of the samples were carried out using a scanning electron microscope (Zeiss Supra 35, Zeiss, Oberkochen, Germany) with a field emission gun. The SEM was equipped with a TEAM™ Trident Analysis system. Secondary electron imaging and energy-dispersive X-ray spectroscopy (EDS) were used to determine the morphology of the samples. Transmission electron microscopy was performed using a S/TEM Titan 80-300 (FEI, Hillsboro, Oregon, UK) working at an accelerating voltage of 300 kV and equipped with EDS detector.

Thermogravimetric analysis of the HKUST-1 and Ce@HKUST-1 was performed using a Mettler-Toledo apparatus (Columbus, Ohio, USA). The loss of sample mass was registered during analyses conducted in flowing air at a temperature increasing from 25 °C to 900 °C with a heating rate of 10 °C/min.

3.4. Catalytic Tests of CO Oxidation

The activity of HKUST-1 and Ce@HKUST-1 in the reaction of CO oxidation was determined at temperatures ranging 140 to 220 °C. The catalyst bed was placed in a quartz reactor and heated up to the given temperature in flowing Ar, with a heating rate of 5 °C/min. Then, a reaction mixture consisting of 1 vol.% CO and 5 vol.% O_2 in Ar was introduced. After at least 3 h of testing under isothermal conditions, the temperature was decreased by 10 °C. The tests were conducted at the gas hourly space velocity GHSV = 10000 h^{-1}. The CO, CO_2, and O_2 concentrations at the reactor outlet

were determined by gas chromatograph. The CO conversion was calculated both from CO consumed and CO_2 produced.

4. Conclusions

In this work, a series of HKUST-1 and Ce@HKUST-1 catalysts was synthesised and tested in the reaction of CO oxidation at temperatures ranging from 140 to 210 °C. The HKUST-1 was obtained both in solvothermal and CTAB-assisted syntheses, whereas the cerium phase was deposited by applying wet and incipient wetness impregnation methods. Our study revealed that the synthesis method of HKUST-1 has a significant impact on its morphology, surface area, and thermal stability. From a chemical point of view, the obtained structures were identical, i.e., they contained both Cu^{2+} and Cu^+ ions, and —in the case of the cerium-loaded samples —had Ce^{4+} and Ce^{3+} ions. However, some impact of the synthesis method on the Cu^{2+}/Cu^+ ratio was observed. It was determined with EDS that cerium deposition over HKUST-1 obtained in the presence of CTAB (either via wet or the IWI method) was more efficient, since CTA^+ could be partially exchanged with cerium. Moreover, cerium deposition over HKUST-1 structures obtained both via the solvothermal and CTAB-assisted routes resulted in an increase in the concentration of Cu^+ ions owing to oxygen transfer from Cu^{2+} to Ce^{3+}, and indicating strong interactions between the Cu nodes in HKUST-1 with deposited Ce species. The negative aspect of such a strong Cu–Ce interaction could be decreased thermal stability under the reaction conditions compared to HKUST-1 samples. This phenomenon was more pronounced for catalysts supported on HKUST-1 obtained using CTAB-assisted synthesis due to the aforementioned partial exchange of CTA^+ to Ce. The reduced surface area of the Ce@H1_CTAB catalysts could also play a role in reduced CO conversion. According to the obtained results, the best catalytic performance revealed the catalytic system composed of nanorods of CeO_x evenly distributed over high surface area HKUST-1, which was obtained using the IWI method. This allowed for the achievement of a good compromise between the physicochemical properties of Ce@HKUST-1, i.e., the uniform CeO_x dispersion over HKUST-1, good CeO_x contact with Cu clusters, sufficient surface area, and relatively high thermal stability, with its catalytic activity in CO oxidation.

References

1. Chui, S.S.; Lo, S.M.; Charmant, J.P.; Orpen, A.G.; Williams, I.D. A Chemically Functionalizable Nanoporous Material [Cu₃(TMA)₂(H₂O)₃]ₙ. *Science* **1999**, *283*, 1148–1150. [CrossRef] [PubMed]
2. Lin, K.-S.; Adhikari, A.K.; Ku, C.-N.; Chiang, C.-L.; Kuo, H. Synthesis and characterization of porous HKUST-1 metal organic frameworks for hydrogen storage. *Int. J. Hydrog. Energy* **2012**, *37*, 13865–13871. [CrossRef]
3. Rungtaweevoranit, B.; Zhao, Y.; Choi, K.M.; Yaghi, O.M. Cooperative effects at the interface of nanocrystalline metal–organic frameworks. *Nano Res.* **2016**, *9*, 47–58. [CrossRef]
4. Tsuruoka, T.; Furukawa, S.; Takashima, Y.; Yoshida, K.; Isoda, S.; Kitagawa, S. Nanoporous Nanorods Fabricated by Coordination Modulation and Oriented Attachment Growth. *Angew. Chem. Int. Ed.* **2009**, *48*, 4739–4743. [CrossRef] [PubMed]
5. Umemura, A.; Diring, S.; Furukawa, S.; Uehara, H.; Tsuruoka, T.; Kitagawa, S. Morphology Design of Porous Coordination Polymer Crystals by Coordination Modulation. *J. Am. Chem. Soc.* **2011**, *133*, 15506–15513. [CrossRef] [PubMed]

6. Schaate, A.; Roy, P.; Godt, A.; Lippke, J.; Waltz, F.; Wiebcke, M.; Behrens, P. Modulated Synthesis of Zr-Based Metal-Organic Frameworks: From Nano to Single Crystals. *Chem. Eur. J.* **2011**, *17*, 6643–6651. [CrossRef]

7. Lu, G.; Cui, C.; Zhang, W.; Liu, Y.; Huo, F. Synthesis and Self-Assembly of Monodispersed Metal-Organic Framework Microcrystals. *Chem. Asian J.* **2012**, *8*, 69–72. [CrossRef]

8. Wißmann, G.; Schaate, A.; Lilienthal, S.; Bremer, I.; Schneider, A.M.; Behrens, P. Modulated synthesis of Zr-fumarate MOF. *Microporous Mesoporous Mater.* **2012**, *152*, 64–70. [CrossRef]

9. Cravillon, J.; Nayuk, R.; Springer, S.; Feldhoff, A.; Huber, K.; Wiebcke, M. Controlling Zeolitic Imidazolate Framework Nano- and Microcrystal Formation: Insight into Crystal Growth by Time-Resolved In Situ Static Light Scattering. *Chem. Mater.* **2011**, *23*, 2130–2141. [CrossRef]

10. Xin, C.; Zhan, H.; Huang, X.; Li, H.; Zhao, N.; Xiao, F.; Wei, W.; Sun, Y. Effect of various alkaline agents on the size and morphology of nano-sized HKUST-1 for CO_2 adsorption. *RSC Adv.* **2015**, *5*, 27901–27911. [CrossRef]

11. Mu, X.; Chen, Y.; Lester, E.; Wu, T. Optimized synthesis of nano-scale high quality HKUST-1 under mild conditions and its application in CO_2 capture. *Microporous Mesoporous Mater.* **2018**, *270*, 249–257. [CrossRef]

12. Liu, Q.; Jin, L.-N.; Sun, W.-Y. Facile fabrication and adsorption property of a nano/microporous coordination polymer with controllable size and morphology. *Chem. Commun.* **2012**, *48*, 8814–8816. [CrossRef] [PubMed]

13. Nune, S.K.; Thallapally, P.K.; Dohnalkova, A.; Wang, C.; Liu, J.; Exarhos, G.J. Synthesis and properties of nano zeolitic imidazolate frameworks. *Chem. Commun.* **2010**, *46*, 4878–4880. [CrossRef] [PubMed]

14. Sun, Y.; Amsler, M.; Goedecker, S.; Caravella, A.; Yoshida, M.; Kato, M. Surfactant-assisted synthesis of large Cu-BTC MOFs single crystals and the potential utilization as photodetectors. *CrystEngComm* **2019**, *21*, 3948–3953. [CrossRef]

15. Ranft, A.; Betzler, S.B.; Haase, F.; Lotsch, B.V. Additive-mediated size control of MOF nanoparticles. *CrystEngComm* **2013**, *15*, 9296–9300. [CrossRef]

16. Goyal, P.S.; Aswal, V.K. Micellar structure and inter-micelle interactions in micellar solutions: Results of small angle neutron scattering studies. *Curr. Sci.* **2001**, *80*, 972–979.

17. Tan, Y.C.; Zeng, H.C. Defect Creation in HKUST-1 via Molecular Imprinting: Attaining Anionic Framework Property and Mesoporosity for Cation Exchange Applications. *Adv. Funct. Mater.* **2017**, *27*, 1703765. [CrossRef]

18. Wang, F.; Guo, H.; Chai, Y.; Li, Y.; Liu, C. The controlled regulation of morphology and size of HKUST-1 by coordination modulation method. *Microporous Mesoporous Mater.* **2013**, *173*, 181–188. [CrossRef]

19. Isaeva, V.I.; Kustov, L.M. The application of metal-organic frameworks in catalysis (Review). *Pet. Chem.* **2010**, *50*, 167–180. [CrossRef]

20. Yepez, R.; García, S.; Schachat, P.; Sánchez-Sánchez, M.; González-Estefan, J.H.; González-Zamora, E.; Ibrara, I.A.; Aguilar-Pliego, J. Catalytic activity of HKUST-1 in the oxidation of trans-ferulic acid to vanillin. *New J. Chem.* **2015**, *39*, 5112–5115. [CrossRef]

21. Arzehgar, Z.; Sajjadifar, S.; Arandiyan, H. HKUST-1 as an efficient and reusable heterogeneous catalyst for synthesis of 1,4-dihydropyridine at room temperature. *Asian J. Green Chem.* **2018**, *3*, 43–52. [CrossRef]

22. Toyao, T.; Styles, M.J.; Yago, T.; Sadiq, M.M.; Riccò, R.; Suzuki, K.; Horiuchi, Y.; Takahashi, M.; Falcaro, P. Fe_3O_4@HKUST-1 and Pd/Fe_3O_4@HKUST-1 as magnetically recyclable catalysts prepared via conversion from a Cu-based ceramic. *CrystEngComm* **2017**, *19*, 4201–4210. [CrossRef]

23. Guo, P.; Froese, C.; Fu, Q.; Chen, Y.-T.; Peng, B.; Kleist, W.; Fischer, R.A.; Muhler, M.; Wang, Y. CuPd Mixed-Metal HKUST-1 as Catalyst for Aerobic Alcohol Oxidation. *J. Phys. Chem. C* **2018**, *122*, 21433–21440. [CrossRef]

24. Ye, J.; Liu, C. $Cu_3(BTC)_2$: CO oxidation over MOF based catalysts. *Chem. Commun.* **2011**, *47*, 2167–2169. [CrossRef] [PubMed]

25. Zamaro, J.M.; Pérez, N.C.; Miró, E.E.; Casado, C.; Seoane, B.; Téllez, C.; Coronas, J. HKUST-1 MOF: A matrix to synthesize CuO and CuO–CeO_2 nanoparticle catalysts for CO oxidation. *Chem. Eng. J.* **2012**, *195-196*, 180–187. [CrossRef]

26. Zheng, X.-C.; Wu, S.-H.; Wang, S.-P.; Wang, S.-R.; Zhang, S.-M.; Huang, W.-P. The preparation and catalytic behavior of copper–cerium oxide catalysts for low-temperature carbon monoxide oxidation. *Appl. Catal. A Gen.* **2005**, *283*, 217–223. [CrossRef]

27. Lin, K.-S.; Chowdhury, S. Synthesis, Characterization, and Application of 1-D Cerium Oxide Nanomaterials: A Review. *Int. J. Mol. Sci.* **2010**, *11*, 3226–3251. [CrossRef]

28. Goworek, J.; Kierys, A.; Gac, W.; Borówka, A.; Kusak, R. Thermal degradation of CTAB in as-synthesized MCM-41. *J. Therm. Anal. Calorim.* **2009**, *96*, 375–382. [CrossRef]

29. Chitsaz, A.; Jalilpour, M.; Fathalilou, M. Effects of PVP and CTAB surfactants on the morphology of cerium oxide nanoparticles synthesized via co-precipitation method. *Int. J. Mater. Res.* **2013**, *104*, 511–514. [CrossRef]

30. Kim, Y.-Y.; Neudeck, C.; Walsh, D. Biopolymer templating as synthetic route to functional metal oxide nanoparticles and porous sponges. *Polym. Chem.* **2010**, *1*, 272–275. [CrossRef]

31. Pan, C.; Zhang, D.; Shi, L. CTAB assisted hydrothermal synthesis, controlled conversion and CO oxidation properties of CeO_2 nanoplates, nanotubes, and nanorods. *J. Solid State Chem.* **2008**, *181*, 1298–1306. [CrossRef]

32. Peng, B.; Feng, C.; Liu, S.; Zhang, R. Synthesis of CuO catalyst derived from HKUST-1 temple for the low-temperature NH_3-SCR process. *Catal. Today* **2018**, *314*, 122–128. [CrossRef]

33. Fan, C.; Dong, H.; Liang, Y.; Yang, J.; Tang, G.; Zhang, W.; Cao, Y. Sustainable synthesis of HKUST-1 and its composite by biocompatible ionic liquid for enhancing visible-light photocatalytic performance. *J. Clean. Prod.* **2019**, *208*, 353–362. [CrossRef]

34. Hsu, K.; Chen, D. Green synthesis and synergistic catalytic effect of Ag/reduced graphene oxide nanocomposite. *Nanoscale Res. Lett.* **2014**, *9*, 484. [CrossRef]

35. Zhou, L.; Niu, Z.; Jin, X.; Tang, L.; Zhu, L. Effect of Lithium Doping on the Structures and CO_2 Adsorption Properties of Metal-Organic Frameworks HKUST-1. *ChemistrySelect* **2018**, *3*, 12865–12870. [CrossRef]

36. Kozachuk, O.; Yusenko, K.; Noei, H.; Wang, Y.; Walleck, S.; Glaser, T.; Fischer, R.A. Solvothermal growth of a ruthenium metal–organic framework featuring HKUST-1 structure type as thin films on oxide surfaces. *Chem. Commun.* **2011**, *47*, 8509–8511. [CrossRef]

37. Kettner, M.; Ševčíková, K.; Homola, P.; Matolín, V.; Nehasil, V. Influence of the Ce–F interaction on cerium photoelectron spectra in CeOXFY layers. *Chem. Phys. Lett.* **2015**, *639*, 126–130. [CrossRef]

38. Seo, Y.-K.; Hundal, G.; Jang, I.T.; Hwang, Y.K.; Jun, C.-H.; Chang, J.-S. Microwave Synthesis of Hybrid Inorganic−Organic Materials Including Porous $Cu_3(BTC)_2$ from Cu(II)-Trimesate Mixture. *Microporous Mesoporous Mater.* **2009**, *119*, 331–337. [CrossRef]

39. Zhu, C.; Zhang, Z.; Wang, B.; Chen, Y.; Wang, H.; Chen, X.; Zhang, H.; Sun, N.; Wei, W.; Sun, Y. Synthesis of HKUST-1#MCF compositing materials for CO_2 adsorption. *Microporous Mesoporous Mater.* **2016**, *226*, 476–481. [CrossRef]

40. Lin, A.K.-Y.; Hsieh, Y.-T. Copper-based metal organic framework (MOF), HKUST-1, as an efficient adsorbent to remove p-nitrophenol from water. *J. Taiwan Inst. Chem. Eng.* **2015**, *50*, 223–228. [CrossRef]

41. Guo, Z.; Song, L.; Xu, T.; Gao, D.; Li, C.; Hu, X.; Chen, G. CeO_2-CuO Bimetal Oxides Derived from Ce-based MOF and Their Difference in Catalytic Activities for CO Oxidation. *Mater. Chem. Phys.* **2019**, *226*, 338–343. [CrossRef]

42. Zhu, C.; Ding, T.; Gao, W.; Ma, K.; Tian, Y.; Li, X. CuO/CeO_2 catalysts synthesized from Ce-UiO-66 metal-organic framework for preferential CO oxidation. *Int. J. Hydrog. Energy* **2017**, *42*, 17457–17465. [CrossRef]

43. Liu, W.; Stephanopoulos, M.F. Total Oxidation of Carbon Monoxide and Methane over Transition Metal Fluorite Oxide Composite Catalysts: I. Catalyst Composition and Activity. *J. Catal.* **1995**, *153*, 304. [CrossRef]

44. Zhao, F.; Li, S.; Wu, X.; Yue, R.; Li, W.; Zha, X.; Deng, Y.; Chen, Y. Catalytic Behaviour of Flame-Made CuO-CeO2 Nanocatalysts in Efficient CO Oxidation. *Catalysts* **2019**, *9*, 256. [CrossRef]

45. Noei, H.; Amirjalayer, S.; Müller, M.; Zhang, X.; Schmid, R.; Muhler, M.; Fischer, R.A.; Wang, Y. Low-Temperature CO Oxidation over Cu-Based Metal-Organic Frameworks Monitored by using FTIR Spectroscopy. *ChemCatChem* **2012**, *4*, 755–759. [CrossRef]

46. Noei, H.; Kozachuk, O.; Amirjalayer, S.; Bureekaew, S.; Kauer, M.; Schmid, R.; Marler, B.; Muhler, M.; Fischer, R.A.; Wang, Y. CO Adsorption on a Mixed-Valence Ruthenium Metal–Organic Framework Studied by UHV-FTIR Spectroscopy and DFT Calculations. *J. Phys. Chem. C* **2013**, *117*, 5658–5666. [CrossRef]